Research Article

A DISCRETE ELEMENT MODELING INVESTIGATION OF THE CENTRIFUGAL SEPARATION PROCESS OF BOVINE MILK SOMATIC CELLS

Orçun EKİN*[1], Yunus ÇERÇİ[2]

[1]*Aydın Adnan Menderes University, Mechanical Engineering Dept., AYDIN;* ORCID: 0000-0002-6779-885X
[2]*Aydın Adnan Menderes University, Mechanical Engineering Dept., AYDIN;* ORCID: 0000-0002-4462-5366

ABSTRACT

Number of somatic cells (white blood cells) in bovine milk matrix is one of the defining characteristics of milk quality. An increasing Somatic Cell Count (SCC) in milk negatively effects the texture, color and taste of the substance, reducing its shelf life, hence the commercial value. With somatic cells being considered as sparse particles in a continuous medium, disk-stack centrifuges have become the most common industrial application of reducing and controlling the SCC index. In this study, a Computational Fluid Dynamics-Discrete Element Modeling (CFD-DEM) mainframe on Euler-Lagrange coupling basis is developed to determine the separation ability of a clarifying disk-stack centrifuge. The 3D model is simplified from an actual machine while strictly adopting the geometrical features of the disc-stack. The CFD-DEM model yields a 3.76% relative error in separation ability at average particle diameter, when compared to field tests of the machine at steady operation. Simulations show an increasing g-force, combined with reduced feed rates yields the best separation ability for the process. With optimum process parameters generating a 91.05% sedimentation ratio, the upper limit of g-force at 10 ton/h feed rate offers a 95% separation efficiency, while the lower limit of feed rate offers 96% at 7,700rpm.

Keywords: Centrifugal separation, Euler-Lagrange Coupling, CFD-DEM, bovine milk, somatic cells.

1. INTRODUCTION

Solid bowl centrifuges can be designed and operated both for batch and continuous process. Yet the majority of applications emphasize their ability to separate particles of a large scale without any clogging problems in continuous operation. Disk-stack centrifuges are the most common types of continuously operated solid-bowl centrifuges. Particle-laden medium is fed to the bowl volume, accelerated immediately to the angular velocity maintained, where particles, due to their higher density, forced outwards to the solid walls. Particles sedimented against a solid containing volume, where the sludge is discharged either at intervals (drop-bottom) or continuously, depending on the machine design. Earlier studies on disk-stack centrifuges usually tend to focus on the behavior of particles confined or suspended in a continuous fluid, in a pure mathematical way by employing principal physics. In retrospect, the Stokes' law [1] was the first

---

* Corresponding Author: e-mail: orkun.ekin@adu.edu.tr, tel: (256) 213 75 03 / 3729

physical cornerstone ever to have been employed toward explaining the sedimentation of particles suspended in a medium. This idea introduced the terminal velocity concept into sedimentation of solid particles in a medium. For design, estimation and scale-up purposes, the preliminary research on the sedimentation phenomenon has been satisfactory. Therefore, many product assessments by prominent manufacturers around the globe were earlier performed based on this de facto.

A finite element analysis assuming a simplified model of a commercial centrifugal milk clarifier as the control volume, in terms of somatic cell separation, is investigated in this study. An Euler-Lagrange discrete element model is developed, then a variety of different operation and boundary conditions are employed to understand the particle-laden flow behavior within centrifugal field, via Computational Fluid Dynamics-Discrete Element Modeling (CFD-DEM) approach, after the principal 3D model is validated against field tests conducted on the actual, equivalent machine.

The engineering applications of Stokes' law and terminal velocity concept are often nested with computational methods han dled for specific problems. Studies involving sedimentation behavior of particles incline to solve the transportation character of numerous particles in a continuous medium. Analytically solving force balances for many suspended particles, without computational methods, involve great verbosity, especially when total mass of discrete phase becomes dominant over continuous phase. Kartushinsky et al. [2], inspected the terminal velocities of suspended particles in pipe flows with different characteristics. Implementing the model by using Eulerian schemes for both continuous medium and particles, flow direction and mass concentration effects on particle distributions and axial velocities of both phases are investigated. The difference between the settling velocities of phases is observed to approach to zero, therefore an alternative drag force definition is suggested to regulate the axial component of momentum equation. In their study, Náraigh and Barros [3] discussed the flow of a suspension through an inclined channel. By applying a pressure drop throughout the channel and sustaining a laminar-steady state flow, gravitational/inertial effects on the suspension is investigated. A novel diffuse-flux model is suggested to admit the particle properties better into the modeling equations and allow for a more detailed parameter study on Stokes' force balance in inclined channels. Akbarzadeh and Hrymak [4] investigated both the solid-solid and solid-liquid interaction in a rectangular duct with Poiseuille and Couette formulated flows. Handling particle collision equations, hydrodynamic, thermophoretic forces within a two-way coupling scheme. Particle residence times are investigated when both phases have close length scales, i.e. with unit Reynolds and Stokes numbers. Zhang and Chen [5] investigated the two modeling methods to predict particle behavior in ventilated environments in their study. To handle the workload of continuous medium, the Standard k-ε turbulence model is utilized. First Eulerian, then Lagrangian particle tracking results obtained, then compared with experimental data. Saidi et al. [6] investigated the scatter, settling and accumulation behavior of particles in gaseous phase during inhalation process and through lung alveoli. In many cases though, the particulate phase is scarce when compared to continuous medium; a state where the Lagrangian approach becomes prominent. In applications such as Arsalanloo and Abbasalizadeh [7] suggested, the Eulerian algorithm is utilized to simulate the continuous fluid where the Lagrangian method handles the particulate phase simultaneously to harness the competence of Euler-Lagrange coupling. Euler-Lagrange coupling can be extended to inspect also heat transfer phenomena within particle laden flows. Towards this scenario, Maskaniyan et al. [8] in their paper investigated the discrete characteristics of Al_2O_3 particles in a channel, equipped with a feature with elevated temperatures. Also in a recent study of Chang et al. [9], a 3-D simulation of particle settlement in inclined vessels by implementing an Euler-Lagrange coupling is presented. It is shown that the occurrence of turbulence through the vessels actively reduce the settling behavior of discrete particles where particle size, hence particle inertia becomes significant on a particles fate. Kempken et al. [10] in their study, considered a Westfalia prototype disk-stack centrifuge and tested it to inspect the

mammalian cell sedimentation ability . Experiments were conducted via cell counting and comparison of examples from inlet and outlet streamlines of machinery. Analyses give insight at a certain extent, due to filtration capacity of device utilized to determine the particle sizes on both streams which, as implied in the study, is reliable between 1-5 μm. Lindner et al. [11]. Without revealing the specifics about the CFD-DEM algorithm or the particle-laden flow characteristics, several numerical studies using water and air as continuous media are investigated for a solid bowl centrifuge. A two-way turbulence coupling is implemented to discuss about the particles' effect on the continuous media. Instead of running the Lagrangian equations on a pseudo-transient scheme, the researchers prefer to perform simulations on a completely transient model. Shekhawat et al. [12] investigated the separation performance and production of Therapeutic Monoclonal Antibodies (mAb's). In regular clarifying applications, the fate of the sedimented particles are not considered. Although when it comes to 'harvest' cells from inside the fluid region, cells viability against abrupt centrifugal field becomes the most important constraint. An Eulerian-Eulerian model is implemented where the researchers used Gidaspow drag model [13] to better realize the stresses generated on the particles. A standard k-ε model is selected to simulate the continuous medium. The study offers an empirical approach and to relate the theoretical cell break-up rate to turbulence effects due to centrifugal forces.

Studies in literature focusing on the multi-component flow in centrifugal separators are scarce. Compounded with the specifics of centrifugal machinery and CFD-DEM mainframe as the way of investigation, this field of research represents a promising plane for detailed research. The current study aims to contribute to this field by suggesting a well-established Euler-Lagrange model governed by easy-to-access computer-aided engineering interfaces. Although the study assumes somatic cell separation as a basis, it is easily applicable to any particulate flow through centrifugal machinery.

In the following pages, the implementation of a 3D CFD-DEM model designed and improved for somatic-cell clarification from bovine milk is detailed with results harvested from a variety of operating conditions. A summarized description regarding the physics of turbulence modeling and discrete particle handling through centrifugal field within the machinery, related to the available formulae in literature is presented. The validation of the proposed model against field data obtained by process tests is given in conjunction with particle size distribution assumed from the relevant literature and theoretical equivalent spherical particle calculations.

## 2. THEORETICAL CONSIDERATIONS
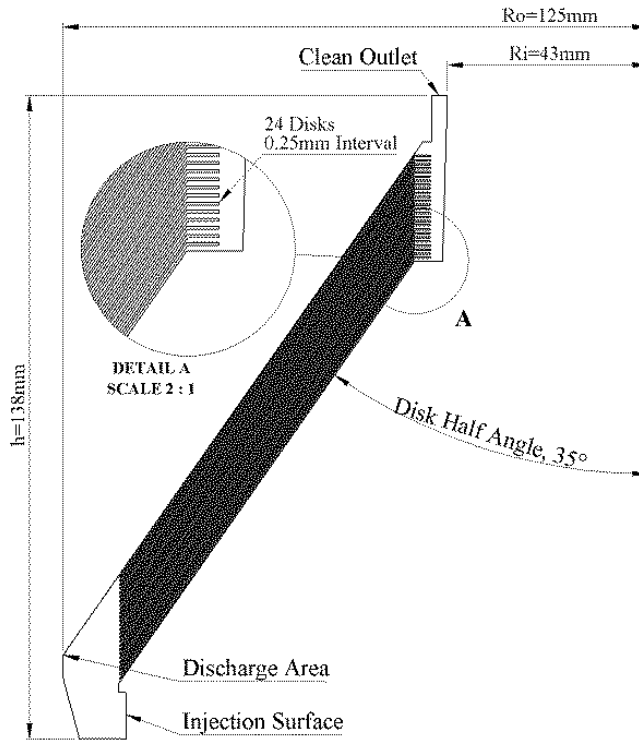
Figure 1. 24-disk bowl representation of two-phase clarifier.

In the scope of this study, a 3-D, rotational region with one inlet and one outlet is considered in a pseudo-transient scenario. As the simplified version of the actual centrifugal separator; the current model involves 24 disks (Figure 1), where all geometric properties of disks were adopted directly from a commercial model of the manufacturer.

A pressure-based solver is preferred, as there is no significant rise (or drop) in temperature during clarifying operation in actual application, hence a change in density. Since the main purpose of a 'two-phase' centrifugal separator is only to prepare milk for successive processes and not to heat-treat the substance; no energy solver model is chosen for this study. In the design operating rate of 7,700 rpm, the centrifugal force reaches 6,640g at the discharge area of the 3-D model. Milk density is assumed to be 1,035 kg/m^3 and viscosity 3.003×10^{-3} Pa.s [14,15] which is constant against changing operating conditions, especially Reynolds number through disks being much lower than that of the rest of the bowl volume.

Steady state scheme is utilized for continuous phase solver, considering the centrifuge must reach to a steady behavior before the examples of 'clarified' milk can be collected. The particles in the centrifugation field are tracked on a time-dependent scheme as they move stochastically [16]. In ANSYS Fluent, this approach to particle-laden flow representation is delivered via a special algorithm called 'unsteady particle tracking' where the a 'time step' in which the particle motion is allowed in simulation calculated in a steady continuous fluid solver [17].
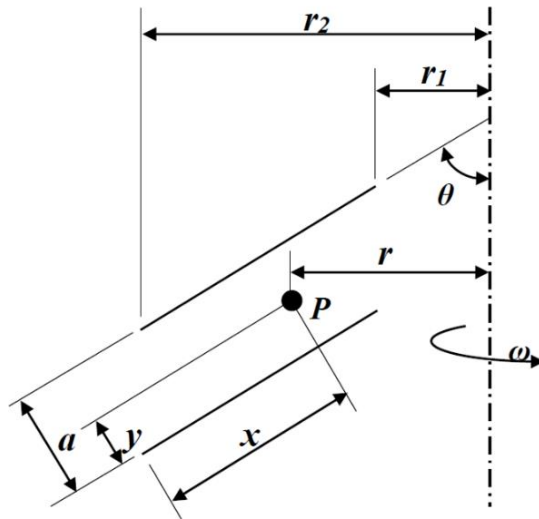
Figure 2. 2D representation of disk-stack; two consecutive disks [18].

A Moving Reference Frame (MRF) is implemented for centrifugal field representation in ANSYS Fluent (Release 17.0). Physical properties of both continuous phase and discrete phase are calculated in a control volume fashion. The problem validation is realized by analyzing the milk against somatic cell count (SCC), the examples of which are collected during milk admission in a diary compound, via fluoro-opto-electronic counting (*ISO 13366-2/AC:2008*) method. Once the model is validated for the optimum operating conditions of the machinery, simulations covering different design aspects are held.

The first sedimentation capability assessment formula was put forward by employing the Stokes' law [18]. When applied to a single particle within a continuous fluid on an inclined channel exposed to centrifugal forces, the Ambler configuration of Stokes' law gives the minimum diameter which can be sedimented out from the volume, that is the unit disk interval (Figure 2).

When disk settler configuration in Fig. 2 is considered, the confined particle "P" is assumed to have settled once it contacts against the wall, that is, the upper disk surface. In this case, the Stoke's velocity and volumetric flow rate depending on the operating conditions and settler geometry can be expressed as in Eqn.s (1) and (2);

$$v_g = \frac{\Delta\rho \, d^2 \, g}{18 \, \mu} \quad [m/s] \tag{1}$$

$$Q = \frac{4\pi \, n \, v_g \, \omega^2}{3gC} (r_2^3 - r_1^3) \, cot\theta \quad [m^3/s] \tag{2}$$

Where $\Delta\rho$ stands for the difference between continuous medium and particle densities, d is particle diameter, n is number of consequent disks in the stack, ω is rotational speed of disk stack, in rad/s and C represents the percentage of the area occupied by flow through the 2-D disk-interval, which is assumed to be '1'. Also the term "cut-off" was first introduced, as a state of operation when half the particles of diameter "d" are sedimented and half escaped to mainstream.

The governing equations of continuity and momentum are expressed for cylindrical coordinates as the separation process essentially takes place inside a revolute-cylindrical geometry. Mass conservation for a flow through a channel exposed to centrifugal processing takes the form in Eqn. (3);

$$\frac{\partial \rho}{\partial t} + \frac{1}{r}\frac{\partial}{\partial r}(r\rho v_r) + \frac{1}{r}\frac{\partial}{\partial \theta}(\rho v_\theta) + \frac{\partial}{\partial z}(\rho v_\theta) = 0 \tag{3}$$

Eqn. (3) involves the three independent orthogonal velocity components, i.e., axial velocity, radial velocity and circumferential velocity, represented by u_z, u_r, u_θ respectively. The circumferential velocity here is positive counterclockwise, that is, in the direction of increasing θ. When we consider the continuous substance –milk is incompressible throughout the process, Eqn. (3) simplifies into Eqn. (4);

$$\frac{1}{r}\frac{\partial}{\partial r}(ru_r) + \frac{1}{r}\frac{\partial}{\partial \theta}(u_\theta) + \frac{\partial}{\partial z}(u_\theta) = 0 \tag{4}$$

As density is constant with regards to time and position whether the flow is steady or unsteady. The resulting equation can be expressed as in Eqn. (5) [19];

$$\nabla \cdot V = 0 \tag{5}$$

For incompressible, isothermal flow (density, ρ=const., viscosity μ=const.), with a velocity field of $\vec{V}$=(u_z, u_r, u_θ), the conservation of momentum equations take the form given below (Eqn.s (6)-(8));

r-component;

$$\rho\left(\frac{\partial u_r}{\partial t} + u_r\frac{\partial u_r}{\partial r} + \frac{u_\theta}{r}\frac{\partial u_r}{\partial \theta} - \frac{u_\theta^2}{r} + u_z\frac{\partial u_r}{\partial z}\right) = -\frac{\partial P}{\partial r} + \rho g_r + \mu\left[\frac{1}{r}\frac{\partial}{\partial r}\left(r\frac{\partial u_r}{\partial r}\right) - \frac{u_r}{r^2} + \frac{1}{r^2}\frac{\partial^2 u_r}{\partial \theta^2} - \frac{2}{r^2}\frac{\partial^2 u_r}{\partial \theta^2} + \frac{\partial^2 u_r}{\partial z^2}\right] \tag{6}$$

z-component;

$$\rho\left(\frac{\partial u_z}{\partial t} + u_r\frac{\partial u_z}{\partial r} + \frac{u_\theta}{r}\frac{\partial u_z}{\partial \theta} + u_z\frac{\partial u_z}{\partial z}\right) = -\frac{\partial P}{\partial z} + \rho g_z + \mu\left[\frac{1}{r}\frac{\partial}{\partial r}\left(r\frac{\partial u_z}{\partial r}\right) + \frac{1}{r^2}\frac{\partial^2 u_z}{\partial \theta^2} + \frac{\partial^2 u_z}{\partial z^2}\right] \tag{7}$$

θ-component;

$$\rho\left(\frac{\partial u_\theta}{\partial t} + u_r\frac{\partial u_\theta}{\partial r} + \frac{u_\theta}{r}\frac{\partial u_\theta}{\partial \theta} + \frac{u_r u_\theta}{r} + u_z\frac{\partial u_\theta}{\partial z}\right) = -\frac{1}{r}\frac{\partial P}{\partial \theta} + \rho g_\theta + \mu\left[\frac{1}{r}\frac{\partial}{\partial r}\left(r\frac{\partial u_\theta}{\partial r}\right) - \frac{u_\theta}{r^2} + \frac{1}{r^2}\frac{\partial^2 u_\theta}{\partial \theta^2} - \frac{2}{r^2}\frac{\partial u_r}{\partial \theta} + \frac{\partial^2 u_\theta}{\partial z^2}\right] \tag{8}$$

As Reynolds numbers calculated inside the separation volume at steady state conditions implied turbulent flow character for continuous medium, turbulence models are investigated. Although the Standard k-ε model is regarded as the most versatile Reynolds Averaged Navier-Stokes (RANS) method both for academic and commercial use; it is observed after numerous attempts to represent flow better inside the separation field that the Standard $k - \omega$ model grasped the turbulence kinetic energy distribution (k) and particle behavior more conveniently when compared to the Standard k-ε.

In the context of the standard $k - \omega$ model, turbulence kinetic energy, k, and the specific dissipation rate, ω, are obtained from the transport equations in Eqn.s (9) and (10), respectively;

$$\frac{\partial}{\partial t}(\rho k) + \frac{\partial}{\partial x_i}(\rho k u_i) = \frac{\partial}{\partial x_j}\left(\Gamma_k\frac{\partial k}{\partial x_j}\right) + G_k - Y_k + S_k \tag{9}$$

$$\frac{\partial}{\partial t}(\rho \omega) + \frac{\partial}{\partial x_i}(\rho \omega u_i) = \frac{\partial}{\partial x_j}\left(\Gamma_\omega\frac{\partial \omega}{\partial x_j}\right) + G_\omega - Y_\omega + S_\omega \tag{10}$$

where G_k and G_ω represent the turbulence kinetic energy (k) generation and specific dissipation rate (ω) generation, respectively. Γ_k is the effective diffusivity of k and Γ_ω is the effective diffusivity of and ω. Y_k and Y_ω represent the dissipation of k and ω due to turbulence. Finally S_k and S_ω are user-defined coefficients [20]. The additional equations and constants constituting the standard $k - \omega$ model are summarized in Table. 1;

Table 1. List of the governing equations of the standard $k - \omega$ model

Definitions	Model Equations
The effective diffusivities for the $k - \omega$ where σ_k and σ_ω are the turbulent Prandtl numbers for k and ω, respectively.	$\Gamma_k = \mu + \dfrac{\mu_t}{\sigma_k}$ (1) $\Gamma_\omega = \mu + \dfrac{\mu_t}{\sigma_\omega}$ (2)
The turbulent viscosity, μ_t, where α^* is employed to compensate for Low-Re numbers. In Eqn. (14) $Re_t = \dfrac{\rho k}{\mu \omega}$, $R_k = 6$, $\alpha_0^* = 0.024$ and $\beta_i = 0.072$, also for high Re-numbers, $\alpha^* = \alpha_\infty^* = 1$.	$\mu_t = \alpha^* \dfrac{\rho k}{\omega}$ (3) $\alpha^* = \alpha_\infty^* \left(\dfrac{\alpha_0^* + Re_t/R_k}{1 + Re_t/R_k} \right)$ (4)
Production of turbulence kinetic energy (G_k) and the production of specific dissipation rate (G_ω) where,	$G_k = -\rho \overline{u_i' u_j'} \dfrac{\partial u_j}{\partial u_i}$ (5) $G_\omega = \alpha \dfrac{\omega}{k} G_k$ (6) with $\alpha = \dfrac{\alpha_\infty}{\alpha^*} \left(\dfrac{\alpha_0 + Re_t/R_\omega}{1 + Re_t/R_\omega} \right)$ (7)
The dissipation of turbulence kinetic energy (Y_k) function with $\chi_k \equiv \dfrac{1}{\omega^3} \dfrac{\partial k}{\partial x_j} \dfrac{\partial \omega}{\partial x_j}$	$Y_k = \rho \beta^* f_{\beta^*} k\omega$ (8) where $f_{\beta^*} = \begin{cases} 1 & \chi_k \le 0 \\ \dfrac{1+680\chi_k^2}{1+400\chi_k^2} & \chi_k > 0 \end{cases}$ (9)
The auxiliary functions and closure parameters	$\beta^* = \beta_i^* [1 + \xi^* F(M_t)]$ (10) $\beta_i^* = \beta_\infty^* \left(\dfrac{4/15 + \left(Re_t/R_\beta\right)^4}{1 + \left(Re_t/R_\beta\right)^4} \right)$ (11) with $\xi^* = 1.5$, $R_\beta = 8$, $\beta_\infty^* = 0.09$
The dissipation of ω is given by in Eqn. (22) where the parameters β_i^* and $F(M_t)$ are defined by Eqn. (21) and Eqn. (27), respectively.	$Y_\omega = \rho \beta f_\beta \omega^2$ (12) where $f_\beta = \dfrac{1+70\chi_\omega}{1+80\chi_\omega}$ (13) $\chi_\omega = \left| \dfrac{\Omega_{ij}\Omega_{jk}\Omega_{ki}}{(\beta_\infty^* \omega)^3} \right|$ (14) $\Omega_{ij} = \dfrac{1}{2} \left(\dfrac{\partial u_i}{\partial x_j} - \dfrac{\partial u_j}{\partial x_i} \right)$ (15) $\beta = \beta_i \left[1 - \dfrac{\beta_i^*}{\beta_i} \xi^* F(M_t) \right]$ (16)
The compressibility function, $F(M_t)$ for high-Reynolds numbers, $\beta_i^* = \beta_\infty^*$. Also $\beta^* = \beta_i^*$ in the incompressible scheme.	$F(M_t) = \begin{cases} 0 & M_t \le M_{t0} \\ M_t^2 - M_{t0}^2 & M_t > M_{t0} \end{cases}$ (17) with $M_t^2 \equiv \dfrac{2k}{a^2}$, $M_{t0} = 0.25$ and $a = \sqrt{\gamma RT}$
The remaining constants are summarized below. $\alpha_\infty^* = 1$, $\alpha_\infty = 0.52$, $\alpha_0 = 1/9$, $\beta_\infty^* = 0.09$, $\beta_i = 0.072$, $R_\beta = 8$ $R_\beta = 6$, $R_\omega = 2.95$, $\xi^* = 1.5$, $M_{t0} = 0.25$, $\sigma_k = 2.0$, $\sigma_\omega = 2.0$	

The Computational Fluid Dynamics–Discrete Element Modeling (CFD-DEM) framework implemented in this study follows the the Euler-Lagrange approach. The liquid phase is treated as a continuum on which the mesh is fixed, whereas particles are solved by transferring their

physical properties (momentum, mass and energy) from element to element on the Eulerian mesh structure, hence the Lagrangian particle tracking.

Table 2. List of the governing equations for the discrete phase

Definitions	Model Equations	
Force balance on the particle confined in a continuous medium where $\vec{F}$ is an additional acceleration term.	$\dfrac{d\vec{u}_p}{dt} = F_D(\vec{u} - \vec{u}_p) + \dfrac{\vec{g}(\rho_p - \rho)}{\rho_p} + \vec{F}$	(18)
The drag force per unit particle mass $F_D(\vec{u} - \vec{u}_p)$.	$F_D = \dfrac{18\mu}{\rho_p d_p^2} \dfrac{C_D Re}{24}$	(19)
	where, $\vec{u}$ is the fluid phase velocity, $\vec{u}_p$ is the particle velocity, μ is the molecular viscosity of the fluid, ρ is the fluid density, ρ_p is the density of the particle, and d_p is the particle diameter.	
Relative Reynolds number	$Re \equiv \dfrac{\rho d_p \lvert \vec{u}_p - \vec{u} \rvert}{\mu}$	(20)
The additional force term, $\vec{F}$, in Eqn. (28) also includes forces on particles that arise due to rotation of the reference frame, i.e. when a Moving Reference Frame (MRF) is applied.	$\left(1 - \dfrac{\rho}{\rho_p}\right)\Omega^2 x + 2\Omega\left(u_{p,y} - \dfrac{\rho}{\rho_p}u_y\right)$ where $u_{p,y}$ and u_y are the particle and fluid velocities in the Cartesian y direction, Ω is the RPM, and;	(21)
For rotation defined about the z axis, as in our study, the forces on the particles in the remaining Cartesian x- and y- directions can be written as in Eqn.s (31) and (32).	$\left(1 - \dfrac{\rho}{\rho_p}\right)\Omega^2 y + 2\Omega\left(u_{p,x} - \dfrac{\rho}{\rho_p}u_x\right)$ where $u_{p,x}$ and u_x are the particle and fluid velocities in the Cartesian x direction.	(22)

The discrete phase and continuous medium are confined to a one-way interaction (continuous fluid flow affecting the particles). DEM calculations are conducted for every time step of discrete phase, i.e. the particle time step in pseudo-transient solver. The particle trajectories are calculated at every time step by implementing a force balance on every single particle which simply equates particle inertia with the forces acting on the particle. Equations governing particle behavior are summarized in Table 2 [21].
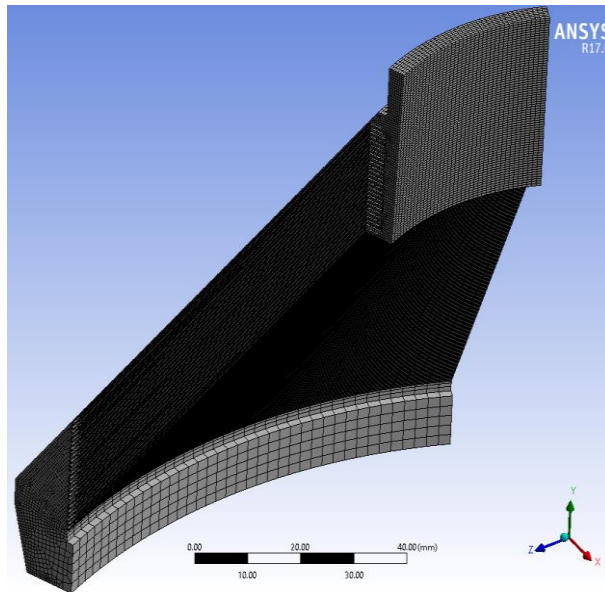
Figure 3. Detail of mesh view, 45° model with 0.25mm disk interval.

Table 2. List of the governing equations for the discrete phase

Definitions	Model Equations	
Force balance on the particle confined in a continuous medium where $\vec{F}$ is an additional acceleration term.	$$\frac{d\vec{u}_p}{dt} = F_D(\vec{u} - \vec{u}_p) + \frac{\vec{g}(\rho_p - \rho)}{\rho_p} + \vec{F}$$	(28)
The drag force per unit particle mass $F_D(\vec{u} - \vec{u}_p)$.	$$F_D = \frac{18\mu}{\rho_p d_p^2} \frac{C_D Re}{24}$$ where, $\vec{u}$ is the fluid phase velocity, $\vec{u}_p$ is the particle velocity, μ is the molecular viscosity of the fluid, ρ is the fluid density, ρ_p is the density of the particle, and d_p is the particle diameter.	(29)
Relative Reynolds number	$$Re \equiv \frac{\rho d_p |\vec{u}_p - \vec{u}|}{\mu}$$	(30)
The additional force term, $\vec{F}$, in Eqn. (28) also includes forces on particles that arise due to rotation of the reference frame, i.e. when a Moving Reference Frame (MRF) is applied.	$$\left(1 - \frac{\rho}{\rho_p}\right)\Omega^2 x + 2\Omega\left(u_{p,y} - \frac{\rho}{\rho_p}u_y\right)$$ where $u_{p,y}$ and u_y are the particle and fluid velocities in the Cartesian y direction, Ω is the angular velocity.	(31)
For rotation defined about the z axis, as in our study, the forces on the particles in the remaining Cartesian x- and y- directions can be written as in Eqn.s (31) and (32).	$$\left(1 - \frac{\rho}{\rho_p}\right)\Omega^2 y + 2\Omega\left(u_{p,x} - \frac{\rho}{\rho_p}u_x\right)$$ where $u_{p,x}$ and u_x are the particle and fluid velocities in the Cartesian x direction.	(32)

A multizone (forced hexahedral) mesh with 600,000 nodes and 345,000 elements is decided after alternative structures implemented to provide convenient results at lower element numbers. Multizone algorithm is preferred due to its ability to keep orthogonality and skewness parameters in check. Also, a three-layer element sizing is applied to disk intervals to better capture the wall boundary layers and a 5x40 element sizing is to fix number of elements -hence, 200 particles are injected on the 'inlet' surface.

Figure 3 gives a detailed view of 0.25mm disk interval geometry with hexahedral mesh. Four typical boundary conditions are available through actual measurements from machinery; pressure readings (typically gage pressures) from input and output, bowl rate and input rate. Again, all these data bound to show slight variations from time to time, as stated before. A complete list of boundary conditions can be seen on Table 3. A 'Wall' indicates any surface either particle or fluid is in contact with.

The particle size range considered is based on an earlier study [22]. The regular number of elements on the inlet surface is adjusted by assigning a 5x40 grid to reduce computational time and effort. This approach was also necessary as the actual SCC index from the field tests required an average 500,000 particles to be modeled at each second of the solver time. Number of particles injected in DEM software is determined directly by the number of elements on the injection surface, unless the particle clouds are considered which, in our case, was out of possibility. Therefore, the injection surface is limited to 200 elements to provide a better aspect ratio on inlet surface of geometry. The DEM properties are detailed on Table 3.

Table 3. Boundary conditions (BC) set for the CFD-DEM model

| Boundary Type	Value	MRF Behavior	DEM Behavior
Wall (Discharge)	No-slip Wall	Rel. to Adj. Cell Zone	Trap
Wall (Other)	No-slip Wall	Rel. to Adj. Cell Zone	Reflect
Mass Flow Inlet	51.7 kg/h	N/A	Reflect
Pressure Outlet	2.2 Bar	N/A	Escape

3. RESULTS AND DISCUSSION

The simplified disk-stack representation to be utilized in the following simulations is prepared by maintaining the exact geometric details, alongside the process parameters like bowl outlet pressure and angular velocity. The only limited feature of the complete disk-stack assembly during CFD translation is indeed the number of disks, hence the throughput rate is reduced accordingly. Locating as many disks as the centrifuge bowl can be stacked up with is the main mechanic of reducing the flow rate between individual disks. This 'filtering' effect of continuous medium generates extremely low flow rates, therefore allowing a laminar flow in the presence of drastic centrifugal forces.
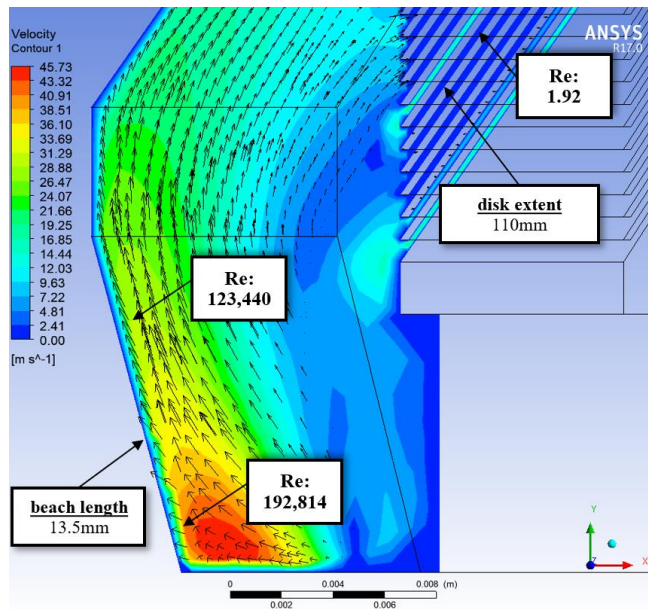
Figure 4. Reynolds number survey near settler beach and through disk interval.

The interruption inside the flow region by the presence of disk-stack also has a side-effect: the otherwise uniform pattern of continuous flow is directly and negatively affected by disk-stack that splits the total throughput into uneven channel flows. We observed that the channels (disk intervals) are either overloaded during the process or there is no significant flow between certain disks. A preliminary analysis on how relative velocity varies through the separation field; both disk-stack and free flow regions (Figure 4). The relative velocities, when the beach length just below the settler area is assumed to be critical length for Reynolds number, displays local Re numbers well above 10^5 level. On the contrary, low-Reynolds numbers can be calculated in the same contour graph, indicating a laminar flow through disk-stack. In terms of pressure distribution through the sedimentation zone (i.e. free-flow zone), the RANS methods show a similar solution on Figure 5. Higher pressure fields between the disks are visible on the geometry (left column, for both methods), that is against the direction of rotation (toward -*y*).

(a)   (b)
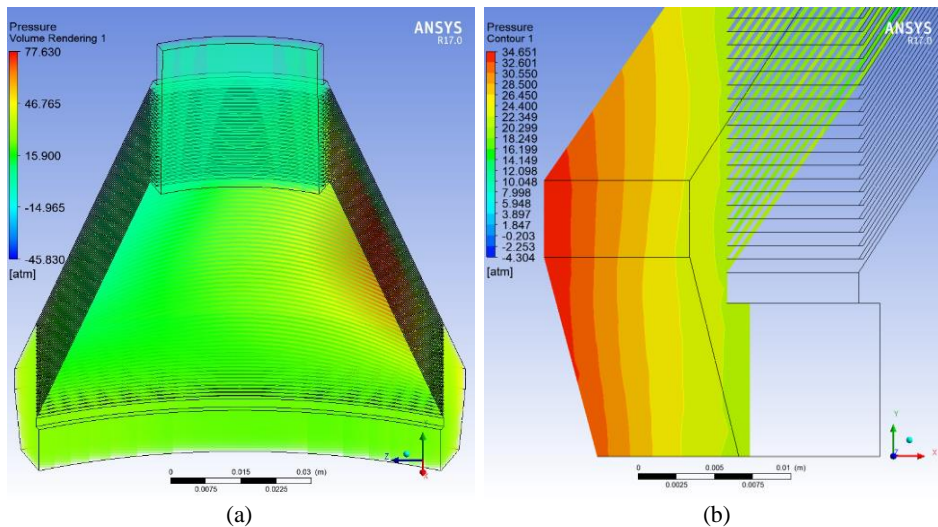
Figure 5. Pressure distribution in the flow region for the Standard $k - \omega$ model with
(a) volume rendering and (b) cross-section view over XY plane.

In steady state operation, the clarifying centrifuge delivers an 87.83% separation performance in steady-state operation. That is, SCC index is dropped from 690,000 on the inlet example of raw milk to 84,000 on the outlet example (Table 4). The measurements were performed by using fluoro-opto-electronic counting (*ISO 13366-2/AC:2008*); a variant of flow cytometry and a popular technology to analyze the characteristics of cells or particles [23,24]. The Standard $k - \omega$ model validates the field test at operation parameters pointed out in problem definition. To control the number of iterations, hence the particle time-steps, the residual criteria are arranged to a 10^{-3} limit for each parameter calculated.

Table 4. Steady-state separation efficiency is validated through CFD-DEM modeling.

RANS	CFD-DEM	Field Test	Rel. Error
RNG k-ε	74.21%	87.83%	15.507%
Standard k-ω	91.05%	87.83%	*3.666%*

Reducing throughput rates allow substance to linger inside the solid-bowl for longer periods of time, exposed to centrifugal forces, therefore increasing the settling ability of an entire range of particles. Fig. 6 shows the relation between throughput rate and sedimentation percentage of the Zlotnik particle size range. Simulations are conducted using the Standard $k - \omega$ model for three alternative throughput rates, 5, 10 and 15 ton/h. Contrary to throughput rates, bowl rate positively affects the separation performance only when increased: centrifugal forces increase with increasing bowl angular speeds. Three variations of bowl rates tested with RNG $k - \varepsilon$ and the Standard $k - \omega$ turbulence models. Due to the better response at the validation point and overall consistency displayed by the Standard $k - \omega$ during the simulations, this turbulence model is assumed for the continuous phase representation in the current study. Detailed results with the Standard $k - \omega$ RANS model can be seen on Figures 6 and 7.
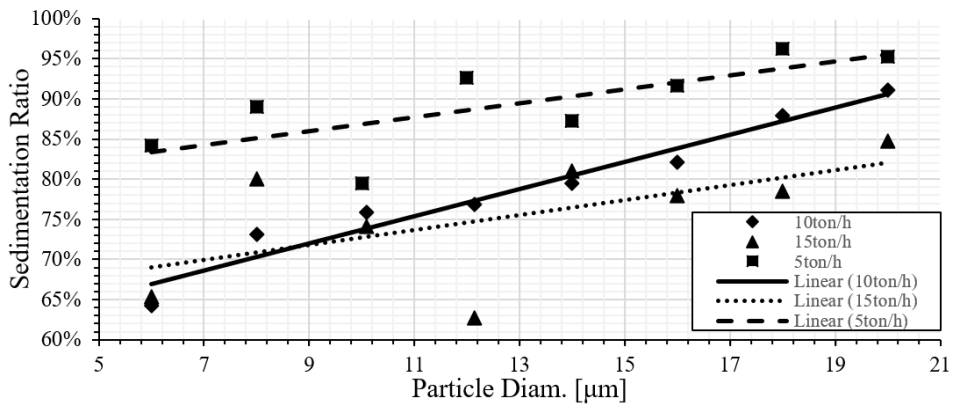
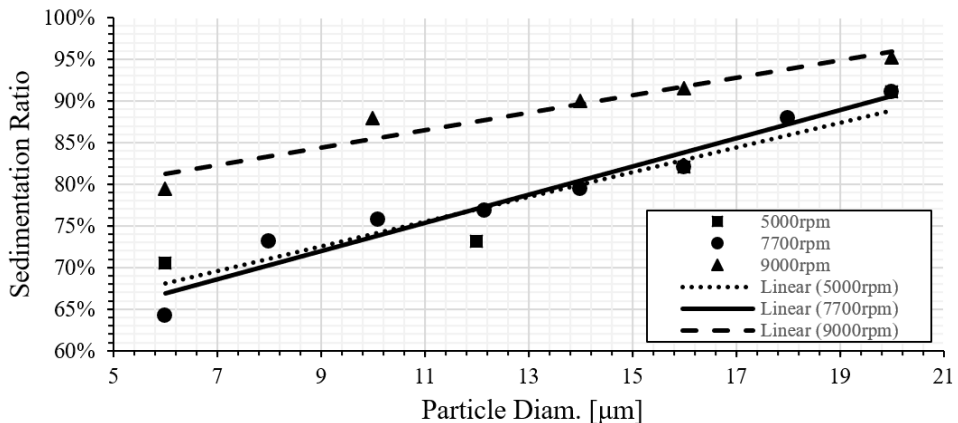**Figure 6.** Sedimentation efficiencies at increasing throughput rates.

Figure 7. Separation efficiencies at increasing bowl rates.

4. CONCLUSION

Results indicate that, increasing diameter of particle, hence the mass of an individual particle causes larger centrifugal forces to act on it, therefore the particles with higher diameters are more prone to sedimentation. At the actual operating rate of 7,700rpm, this tendency increases the particle sedimentation from 66% up to 91%. Also, separation ability of the machine increases with decreasing throughput rate. 5 ton/h is selected as the lower limit of throughput rate. By maintaining all other process and model parameters, lower limit of throughput rate offsets the remaining two options, 10 ton/h (optimal rate) and 15 ton/h, in terms of better sedimentation of particles. It is suggested that when the same setup is operated with higher feed rates to increase mass product, particle sedimentation drops dramatically. This is best represented at a relatively larger particle diameter of 12.2μm approx., where increasing feed rate reduces the separation ratio from 92.5% to 62%. Finally, with higher bowl speeds, the separation efficiency is significantly increased: higher the centrifugal forces, better the chances of sedimentation for particles of every size. With a drastic 15,400g centrifugal force at 9,000rpm, on the other hand, heavier and larger machinery due to power requirements and dynamic loading effects becomes a necessity.

Acknowledgement

NOMENCLATURE

v_g: Particle velocity
ρ_p: Density of discrete particles
ρ_m: Density of continuous medium
μ: Dynamic viscosity
ω, Ω: Angular velocity
N: Revolutions per minute
n: Number of Disks
F_g: Gravitational force

F_b: Buoyancy Force
F_d: Drag Force
ϑ: Stokes' Terminal Velocity
Re: Reynolds Number
Q: Throughput rate
Σ: Centrifuge equivalent surface area
d_{cutoff}: Particle diameter at cut-off
r_2: Disk outer diameter
r_1: Disk inner diameter
θ: Disk half-angle
d_{min}: Minimum particle diameter
d_o: Average particle diameter
$\vec{V}$: Velocity Field for cylindrical coord.

P: Pressure
k: Turbulence kinetic energy
ε: Turbulence dissipation rate
ω: Specific rate of dissipation
α: Inverse effective Prandtl number
$\hat{v}$: Turbulent viscosity $(k - \varepsilon)$
G_k: Turbulent kin. energy generation
G_ω: Specific diss. rate generation

Γ_k: Effective diffusivity of k
Γ_ω: Effective diffusivity of ω
Y_k: Dissipation of k due to turbulence
Y_ω: Dissipation of ω due to turbulence
σ_k: Turbulent Prandtl number for k
σ_ω: Turbulent Prandtl number for ω
μ_t: Turbulent viscosity $(k - \omega)$
α^*: Low-Re buffer coeff. $(k - \omega)$
$F(M_t)$: Compressibility function
$\bar{u}$: Mean fluid phase velocity
T: Integral time scale
T_L: Lagrangian integral time
C: Area occupied by the flow

REFERENCES

[1]   Stokes, G. G. 1851. On the Theories of the Internal Friction of Fluids in Motion, and of the Equilibrium and Motion of Elastic Solids. Mathematical and Physical Papers Vol.1, 9, 75–129. https://doi.org/10.1017/CBO97805117022

[2]   Kartushinsky, A., Tisler, S., Oliveira, J. L. G., and van der Geld, C. W. M. 2016. Eulerian-Eulerian modelling of particle-laden two-phase flow. Powder Technology, *301*, 999–1007. https://doi.org/10.1016/j.powtec.2016.07.053

[3]   Náraigh, L., and Barros, R. 2016. Particle-laden viscous channel flows: Model regularization and parameter study. European Journal of Mechanics, *B/Fluids*, *59*, 90–98. https://doi.org/10.1016/j.euromechflu.2016.05.005

[4]   Akbarzadeh, V., and Hrymak, A. N. 2016. Coupled CFD-DEM of particle-laden flows in a turning flow with a moving wall. Computers and Chemical Engineering, *86*, 184–191. https://doi.org/10.1016/j.compchemeng.2015.12.020

[5]   Zhang, Z., and Chen, Q. 2007. Comparison of the Eulerian and Lagrangian methods for predicting particle transport in enclosed spaces. Atmospheric Environment, *41*(25), 5236–5248. https://doi.org/10.1016/j.atmosenv.-2006.05.086

[6]   Saidi, M. S., Rismanian, M., Monjezi, M., Zendehbad, M., and Fatehiboroujeni, S. 2014. Comparison between Lagrangian and Eulerian approaches in predicting motion of micron-sized particles in laminar flows. Atmospheric Environment, *89*, 199–206. https://doi.org/10.1016/j.atmosenv.2014.01.069

[7]   Arsalanloo, A., and Abbasalizadeh, M. 2017. Numerical study on deposition of particles in a 90° bend in the presence of swirling flow using Eulerian-Lagrangian method. Powder Technology, *320*, 285–294. https://doi.org/10.1016/j.powtec.2017.07.050

[8]   Maskaniyan, M., Rashidi, S., and Esfahani, J. A. 2017. A two-way couple of Eulerian-Lagrangian model for particle transport with different sizes in an obstructed channel. Powder Technology, *312*, 260–269. https://doi.org/10.1016/j.powtec.2017.02.031

[9]   Chang, Y. C., Chiu, T. Y., Hung, C. Y., and Chou, Y. J. 2019. Three-dimensional Eulerian-Lagrangian simulation of particle settling in inclined water columns. Powder Technology, *348*, 80–92. https://doi.org/10.1016/j.powtec.2019.02.052

[10]   Kempken, R., Preissmann, A., and Berthold, W. 1995. Assessment of a disc stack centrifuge for use in mammalian cell separation. Biotechnology and Bioengineering, *46*(2), 132–138. https://doi.org/10.1002/bit.260460206

[11]   Lindner, J., Menzel, K., and Nirschl, H. 2013. Simulation of magnetic suspensions for HGMS using CFD, FEM and DEM modeling. Computers and Chemical Engineering. https://doi.org/10.1016/j.compchemeng.2013.03.012

[12]   Shekhawat, L. K., Sarkar, J., Gupta, R., Hadpe, S., and Rathore, A. S. 2018. Application of CFD in Bioprocessing: Separation of mammalian cells using disc stack centrifuge during production of biotherapeutics. Journal of Biotechnology. https://doi.org/10.1016/j.jbiotec.2017.12.016

[13]   Gidaspow, D. 2012. Multiphase Flow and Fluidization: Continuum and Kinetic Theory Descriptions. Springer International Publishing, ISBN 978-3-319-45490-0, Switzerland.

[14]   Spreer, E. 2017. Milk and Dairy Product Technology. Marcel Dekker, Inc., ISBN 978-0-82-470094-5, NY, United States.

[15]   Wilbey, R. A. 2004. Homogenization of Milk, Encyclopedia of Dairy Sciences. Elsevier Science Ltd., ISBN 978-0-12-374407-4, London, United Kingdom.

[16]   Stolarski, T., Nakasone, Y., and Yoshimoto, S. 2006. Engineering Analysis with ANSYS Software. Elsevier Butterworth-Heinemann, ISBN 978-0-75-066875-X, Oxford, United Kingdom.

[17]   Elghobashi, S. 1994. On predicting particle-laden turbulent flows. Applied Scientific Research. https://doi.org/10.1007/BF00936835

[18]   Ambler, C. M. 1959. The theory of scaling up laboratory data for the sedimentation type centrifuge. Journal of Biochemical and Microbiological Technology and Engineering, *1*(2), 185–205. https://doi.org/10.1002/jbmte.390010206

[19]   White, F. M. 2016. Fluid Mechanics 8th in SI units. McGraw-Hill Education, ISBN 978-9-38-596549-4, NY, United States.

[20]   Versteeg, H.K., Malalasekera, W., 2007. An Introduction to Computational Fluid Dynamics 2e, Pearson Ed. Ltd., ISBN 978-0-13-127498-3, Essex, England.

[21]   ANSYS Inc. 2010. Fluent Theory Guide. Ansys Inc. Southpointe, Canonsburg, PA.

[22]   Zlotnik, I. 1947. Types of Cells Present in Cow's Milk. Journal of Comparative Pathology and Therapeutics, *57*, 196-IN6. https://doi.org/10.1016/s0368-1742(47)80025-6

[23]   Gunasekera, T. S., Veal, D. A., and Attfield, P. V. 2003. Potential for broad applications of flow cytometry and fluorescence techniques in microbiological and somatic cell analyses of milk. International Journal of Food Microbiology. https://doi.org/10.1016/S0168-1605(02)00546-9

[24]   Koess, C., and Hamann, J. 2008. Detection of mastitis in the bovine mammary gland by flow cytometry at early stages. Journal of Dairy Research. https://doi.org/10.1017/s0022029908003245